



1 GUV long-term measurements of total ozone column and effective 2 cloud transmittance at three Norwegian sites

3 Tove M. Svendby¹, Bjørn Johnsen², Arve Kylling¹, Arne Dahlback³, Germar H. Bernhard⁴, Georg H.
4 Hansen¹, Boyan Petkov⁵, Vito Vitale⁵

5 ¹NILU-Norwegian Institute for Air Research, Norway

6 ²Norwegian Radiation and Nuclear Safety Authority, Norway

7 ³University of Oslo, Norway

8 ⁴Biospherical Instruments, Inc., USA

9 ⁵Institute of Atmospheric Sciences and Climate (ISAC) of the Italian National Research Council (CNR), Italy

10 *Correspondence to:* Tove M. Svendby (tms@nilu.no)

11 1. Abstract

12 Measurements of total ozone column and effective cloud transmittance have been performed since 1995 at the three Norwegian
13 sites Oslo/Kjeller, Andøya/Tromsø and in Ny-Ålesund (Svalbard). These sites are a subset of 9 stations included in the
14 Norwegian UV monitoring network, which uses GUV multi-filter instruments and is operated by DSA and NILU. The network
15 includes unique data sets of high time-resolution measurements that can be used for a broad range of atmospheric and biological
16 exposure studies. Comparison of the 25-year records of GUV (global sky) total ozone measurements with Brewer direct sun
17 (DS) measurements show that the GUVs provide valuable supplements to the more standardized ground-based instruments.
18 The GUVs can fill in missing data and extend the measuring season at sites with reduced staff and/or characterized by harsh
19 environmental conditions, such as Ny-Ålesund. Also, a harmonized GUV can easily be moved to more remote/unmanned
20 locations and provide independent total ozone column datasets. The GUV in Ny-Ålesund captured well the Arctic ozone hole
21 in March/April 2020, whereas the GUV in Oslo recorded a mini ozone hole in December 2019 with total ozone values below
22 200 DU. For all the three Norwegian stations there is a slight increase in total ozone from 1995 until today. Measurements of
23 GUV effective cloud transmittance in Ny-Ålesund indicate that there has been a significant change in albedo during the past
24 25 years, most likely resulting from increased temperatures and Arctic ice melt in the area surrounding Svalbard.

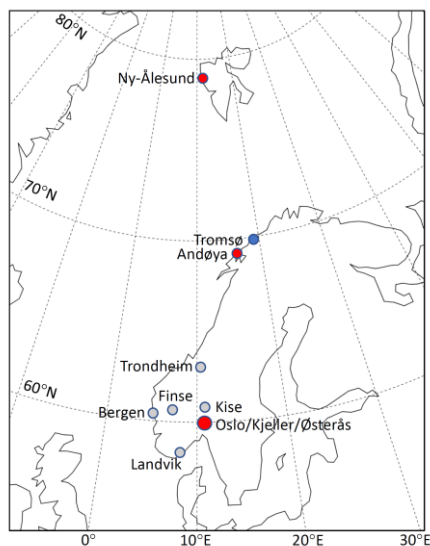
26 2. Introduction

27 The amount of stratospheric ozone decreased significantly both globally and over Norway during the 1980s and 1990s (WMO
28 2018; Svendby and Dahlback, 2004). This decrease was mainly caused by the release of ozone depleting substances (ODSs).
29 In 1987, the Montreal Protocol was signed with the aim of phasing out the production of ODSs. Motivated by this treaty, the
30 Norwegian Environment Agency established the programme “Monitoring of the atmospheric ozone layer” in 1990. Five years



31 later, in 1995/1996, the network was expanded and “*The Norwegian UV network*” was established with funding from the
32 Norwegian Ministry of Health and Care Services and the Norwegian Environment Agency. This network consists of nine
33 Ground-based UltraViolet (GUV) radiometers located at sites between 58°N and 79°N (Figure 1). The network has been in
34 operation for 25 years, and the measurements are undertaken by the Norwegian Radiation and Nuclear Safety Authority, DSA
35 (formerly the Norwegian Radiation Protection Authority, NRPA) and the Norwegian Institute for Air Research (NILU). The
36 GUV instruments allow the calculation of the UV Index, retrievals of total ozone column, cloud transmittance, and several
37 other UV-related dose products (Dahlback, 1996; Høiskar et al., 2003; Bernhard et al., 2005). Data and dose products have
38 been used in several international studies (Bernhard et al, 2013; Bernhard et al, 2015; Schmalwieser et al., 2017; Lakkala et
39 al., 2020; Bernhard et al, 2020), and the data are available at <https://github.com/uvnrpa> and Johnsen et al., (2020).

40



41

42 **Figure 1: The Norwegian UV network. Grey circles represent stations operated by DSA, whereas red circles represent sites operated**
43 **by NILU. The large red circle to the south includes the three stations at Østerås (DSA), Blindern in Oslo, and Kjeller. The**
44 **instrument in Tromsø (blue circle) was moved to Andøya in 2000.**

45

46 The spectral distribution of solar UV radiation reaching the ground depends on the optical properties of the atmosphere, the
47 solar zenith angle (SZA) and reflection from the Earth’s surface. The transmission of solar radiation in the UVB region (280–
48 315 nm) through the stratosphere is primarily determined by the amount of stratospheric ozone, whereas the attenuation in the
49 troposphere is mainly due to scattering by air molecules (Rayleigh scattering), aerosols, and clouds. Generally, a decrease in
50 total ozone column leads to an increase in UVB radiation.

51



52 High-wavelength-resolution spectroradiometers can provide detailed information about the spectral distribution of UV
53 radiation. Stamnes et al. (1991) showed that spectra from such instruments can be used to determine total ozone and cloud
54 transmission accurately. However, simpler and cheaper radiometers with channels in both the UVB and the UVA regions, such
55 as the GUVs, have also demonstrated to be a good alternative to expensive spectroradiometers (Dahlback, 1996; Bernhard et
56 al., 2005; Sztipanov et al., 2020).

57
58 In this study, we present a 25-year time series of total ozone column (TOC) from the Norwegian UV Network. We have
59 focused on three stations operated by NILU located in Oslo/Kjeller, at Andøya/Tromsø and in Ny-Ålesund as shown by red
60 circles in Figure 1. All stations are equipped with additional total ozone measuring instruments such as Brewers
61 spectrophotometers and a Systeme d'Analyse par Observation Zenithale (SAOZ) instrument. TOCs derived from the GUVs
62 are compared to measurements from other ground-based instruments. In addition, they are compared with satellite retrieved
63 data sets. The current work also presents trends in total ozone and effective cloud transmittances.

64

65 **3. Method**

66 **3.1 The GUV instruments in the Norwegian UV network**

67 The GUV is a multi-wavelength filter radiometer manufactured by Biospherical Instruments Inc (BSI), San Diego (Bernhard
68 et al., 2005). The detector unit is environmentally sealed and temperature stabilized, facilitating long-term reliable operation
69 under harsh outdoor conditions. The GUVs have 5 channels in the UV range where each channel has a dedicated filter, a
70 photodetector, and electronics that samples the output at a rate of about 3 Hz. The channels measure simultaneously global
71 (direct and diffuse) solar irradiance at several UV wavelengths, which can be used to "reconstruct" the solar spectrum in the
72 UV range and to compute biological doses, the UV Index, total ozone, and cloud transmittance.

73

74 The UV network consists of 12 multiband filter radiometers (model GUV-541 and GUV-511) (Bernhard et al. 2005). Nine of
75 them are continuously operating at the network locations (Table 1) and three serve calibration purposes and are backups in
76 case of failure at some of the stations. The instrument in Oslo/Kjeller is a GUV-511, whereas the instruments at the other sites
77 are GUV-541. Both instrument types have four channels in the UV region (centre wavelengths 305, 320, 340, and 380 nm). In
78 addition, GUV-541 has a fifth UV channel at 313 nm whereas GUV-511 has a fifth channel for measuring Photosynthetically
79 Active Radiation (PAR: 400-700 nm). The bandwidths of the UV channels are ~10 nm (full width at half-maximum, FWHM).
80 All the instruments are temperature-stabilized at 40°C. Measurements are recorded as 1-minute averages, and for each
81 instrument/site this represents more than 12 million records since the start in 1995.

82



83 The GUV-511 in Oslo was purchased already in 1993 and was installed at the University of Oslo (UiO) to test the instrument
84 performance and to develop appropriate software. In July 2019, this instrument was moved to Kjeller (~18 km East of UiO)
85 due to termination of total ozone/UV activity at the University of Oslo. Similarly, to assure continuation of the GUV time
86 series, the instrument in Tromsø was moved to the Arctic Lidar Observatory for Middle Atmosphere Research (ALOMAR)
87 facility at Andøya in 2000, about 130 km Southwest of Tromsø. Initial studies showed that the ozone climatology is very
88 similar at the two sites (Høiskar et al., 2001), however, the UV level is normally slightly higher at Andøya as the site is located
89 ~50 km South of Tromsø.

90

91 With a few minor exceptions, the GUV instruments have been running continuously since 1995. The GUV at Andøya has been
92 subjected to some problems, most likely caused by an event of water intrusion. In spring 2013 an error with the 380 nm channel
93 was discovered and the instrument was sent to BSI for repair. Two years later, in 2015, the 320 nm channel failed and had to
94 be replaced. During these time periods spare GUV instruments were deployed from the DSA.

95

96 **Table 1: Overview of the locations, instrument types and institutes involved in the Norwegian UV network**

Site	Location	GUV type (serial)	Supporting TOC instruments	Responsible institute
Landvik	58.0° N, 08.5° E	GUV-541		DSA
Blindern, Oslo (1994-2019)	59.9° N, 10.7° E	GUV-511 (no.9222)	Brewer#42	NILU/UiO
Kjeller ¹ (2019→)	60.0° N, 11.0° E	GUV-511 (no.9222)	Brewer#42	NILU
Østerås	60.0° N, 10.6° E	GUV-541, GUV _{vis} -3511 ²		DSA
Bergen	60.4° N, 05.3° E	GUV-541		DSA
Finse	60.6° N, 07.5° E	GUV-541		DSA
Kise	60.8° N, 10.8° E	GUV-541		DSA
Trondheim	63.4° N, 10.4° E	GUV-541		DSA
Andøya (2000 →)	69.3° N, 16.0° E	GUV-541 (no.9276)	Brewer#104	NILU ³
Tromsø ⁴ (1995-1999)	69.7° N, 17.0° E	GUV-541 (no.9276)	Brewer#104	NILU
Ny-Ålesund	78.9° N, 11.9° E	GUV-541 (no.9275)	Brewer#50 ^{5,7} , SAOZ, Pandora ⁶	NILU ⁷

97 ¹ GUV and Brewer#42 were moved from Blindern (University of Oslo) to Kjeller in June 2019

98 ² GUV_{vis}-3511 was installed in 2018

99 ³ The instrument is inspected daily by staff at Alomar, Andøya Space Center

100 ⁴ GUV and Brewer#104 were moved from Tromsø to Andøya in the winter of 1999/2000

101 ⁵ Brewer#50 is operated by ISAC-CNR, Italy

102 ⁶ Pandora measurements started in the spring 2020

103 ⁷ The instrument is inspected daily by staff from the Norwegian Polar institute



104

105 3.2 Calibrations

106 The procedure for calibrating the GUVs is described by Dahlback (1996) and only briefly presented below. When the GUV
107 Teflon diffuser is illuminated by a source, the photodetector transforms the radiation to an electric current which subsequently
108 is converted to a voltage signal. The measured voltage of channel i is

109

$$V_i = k_i \int_0^{\infty} R'_i(\lambda) F(\lambda) d\lambda \approx k_i \sum_{\lambda=0}^{\infty} R'_i(\lambda) F(\lambda) \Delta\lambda \quad (1)$$

110

111 where k_i is a constant (response factor), $R'_i(\lambda)$ is the relative spectral response function for channel i , and $F(\lambda)$ is the spectral
112 irradiance at wavelength λ . During the calibration, the Sun is used as the light source and the irradiance $F(\lambda)$ is measured by a
113 reference radiometer at the same time as the co-located GUV is recording the voltage V_i . The relative spectral response
114 functions for the GUVs were characterized at the optical laboratory of the Norwegian Radiation and Nuclear Safety Authority
115 (DSA). When V_i , $R'_i(\lambda)$, and $F(\lambda)$ are known, one can calculate the constant k_i and the absolute response for channel i : $R_i(\lambda) =$
116 $k_i R'_i(\lambda)$.

117

118 The shape of the solar UV spectrum at the Earth's surface depends mostly on the solar zenith angle (SZA) and the TOC. Thus,
119 the spectral distribution of $R'_i(\lambda)F(\lambda)$ in Eq. (1) will depend on these parameters (Dahlback, 1996). The error in the derived
120 irradiance depends on how much the atmospheric conditions at the time of the measurement differ from those at the time of
121 the absolute calibration. This is discussed in more detail in Chapter 4.

122

123 The calibration procedure described above is normally done during large national or international intercomparison campaigns,
124 where the GUVs are operating synchronously with co-located high-resolution reference spectroradiometers. One of these
125 campaigns was arranged in Oslo in 2005, initiated through the national project "Factors Affecting UV Radiation in Norway"
126 (FARIN) (Johnsen et al., 2008; WMO 2008). Here the GUVs were intercompared with a Bentham spectroradiometer belonging
127 to DSA, which is closely linked to the Quality Assurance of Spectral Ultraviolet Measurements in Europe (QASUME) World
128 travelling reference spectroradiometer. Another large intercomparison campaign, which included the QASUME reference
129 spectroradiometer, was arranged in May/June 2019 (PMOD/WRC, 2019).

130

131 A key factor for the maintenance of a homogenous and stable calibration scale for the network instruments is a system for
132 quality control which accounts for long-term changes in the absolute response factors k_i . In Norway, this is implemented via a
133 dedicated travelling reference GUV-541, which has been transported to the respective stations every summer since 1995. The



134 traveling instrument is set up next to the stationary GUV and synchronous measurements with the two instruments are
135 performed for about one week. DSA is responsible for these annual assessments of drift and determination of correction factors.
136 Assessments of long-term drift for the travelling reference GUV itself are made at the optical laboratory at DSA. Additionally,
137 the travelling reference GUV has been shipped to the manufacturer every one or two years since 1996 for an independent
138 evaluation of long-term drift and for technical services.

139

140 3.3 Total ozone and eCLT retrievals

141 The GUV data products described in this work consist of measurements used in combination with a radiative transfer model
142 (RTM) based on the discrete ordinate method (Stamnes et al., 1988; Dahlback et al., 1991). When solar radiation passes through
143 the atmosphere, a portion of the UVB radiation will be absorbed by ozone. Other fractions of the radiation will be multiple
144 scattered or absorbed by air molecules, aerosols, and clouds (Stamnes et al., 2017). The total ozone column (TOC) is
145 determined from the GUVs by comparing a measured and calculated N-value, where the calculated N-value is derived from
146 the radiative transfer model. The N-value is defined as the ratio of irradiances in two different UV channels, with spectral
147 response functions $R_i(\lambda)$ and $R_j(\lambda)$. One of the channels is sensitive to total ozone whereas the other one is significantly less
148 sensitive. Hence, the N-value is defined as

149

$$N(SZA, TOC) = \frac{\sum_{\lambda=0}^{\infty} R_i(\lambda) F(\lambda, SZA, TOC) \Delta\lambda}{\sum_{\lambda=0}^{\infty} R_j(\lambda) F(\lambda, SZA, TOC) \Delta\lambda} = \frac{V_i}{V_j} \quad (2)$$

150 where $F(\lambda, SZA, TOC)$ is the solar spectral irradiance at wavelength λ , solar zenith angle SZA, and TOC. V_i and V_j are the
151 measured voltages in channel i and j , respectively. In this study the ratio channel(320nm)/channel(305nm) is used for
152 measuring and modelling the N values in Eq. (2). Prior to the measurements, the RTM has been used to create a lookup table
153 of N for all relevant combinations of SZA and TOC, and the GUV TOC is inferred by comparing the measured V_i/V_j and
154 modelled N-values at the given SZA. The N-tables calculated from the RTM are for clear skies, but the table can also be
155 applied to cloudy skies because the effect of clouds on spectral irradiance at 305 nm and 320 nm is quite similar compared to
156 the large effect of ozone (Stamnes et al., 1991).

157

158 To quantify the effects of clouds, aerosols and changing surface albedo, a cloud transmission factor is introduced. It is defined
159 as the measured irradiance at wavelength channel i and solar zenith angle SZA, $F_i(SZA)$, compared to the modelled irradiance
160 at a cloudless and aerosol-free sky with a none-reflecting surface, $F_{ic}(SZA)$. F_{ic} is calculated for the same wavelength and solar
161 zenith angle as the actual measurement F_i , and a channel insensitive to ozone absorption is selected. The estimates of cloud
162 transmission and optical depth are sensitive to ground reflection, implying that an accurate determination of cloud attenuation



163 requires precise knowledge of the surface albedo. Stamnes et al. (1991) introduced the term *effective* cloud transmittance to
164 account for the influence of surface albedo and aerosols on cloud attenuation. The effective cloud transmittance (eCLT) is
165 defined as:

166

$$eCLT(SZA) = 100 \frac{F_i(SZA)}{F_{ic}(SZA)} \quad (3)$$

167

168 In this study, the 340 nm channel has been selected to determine the eCLT. Alternatively, the 380 nm channel can be used.
169 For both wavelengths, the incoming solar radiation is insensitive to ozone, meaning that the eCLT only is sensitive to clouds,
170 aerosols, and the surface albedo. ECLT may be larger than 100% due to multiple scattering of the solar radiation when broken
171 clouds are present and the sun remains unobscured. Furthermore, the presence of snow on the ground enhances the albedo and
172 contributes to an additional multiple scattering. We do not attempt to separate the effects of clouds, aerosols, and albedo here,
173 and the eCLT quantifies the combined influence of the three factors.

174

175 **4. Data analysis**

176 **4.1 Harmonization of total ozone**

177 The N-tables used in the current work, described in the previous chapter, are based on the 320/305 nm wavelength ratio and
178 RTM calculations with the TOMS V7 ozone climatology (McPeters et al., 1996), which describes an idealized altitude profile
179 of temperature, pressure, and ozone. Previous studies have shown that N-tables generated from this atmospheric profile agreed
180 well with ozone values provided by the Dobson spectrophotometer in Oslo during wintertime (Dahlback, 1996). Several other
181 N-tables are created for the GUVs, both for other wavelength ratios (e.g. 320/313 nm and 340/305 nm) and for subarctic
182 summer and subarctic winter profiles (defined by Anderson et al., 1987). The choice of ozone profile in the calculations of N-
183 value lookup tables is especially important for the winter when the SZA is large. Lapeta et al. (2000) found that an inappropriate
184 ozone profile may cause uncertainties up to 10% in the retrieved TOC for $SZA > 75^\circ$. Sensitivity studies from Dahlback (1996)
185 showed that the errors in total ozone, related to an inappropriate atmospheric profile in the RTM, was less than 1% for $SZA <$
186 65° . However, the error could be as large as 30% (at $SZA=80^\circ$) if a subarctic winter profile was replaced with a tropical
187 atmospheric profile. This latter example represents an extreme situation in Norway.

188

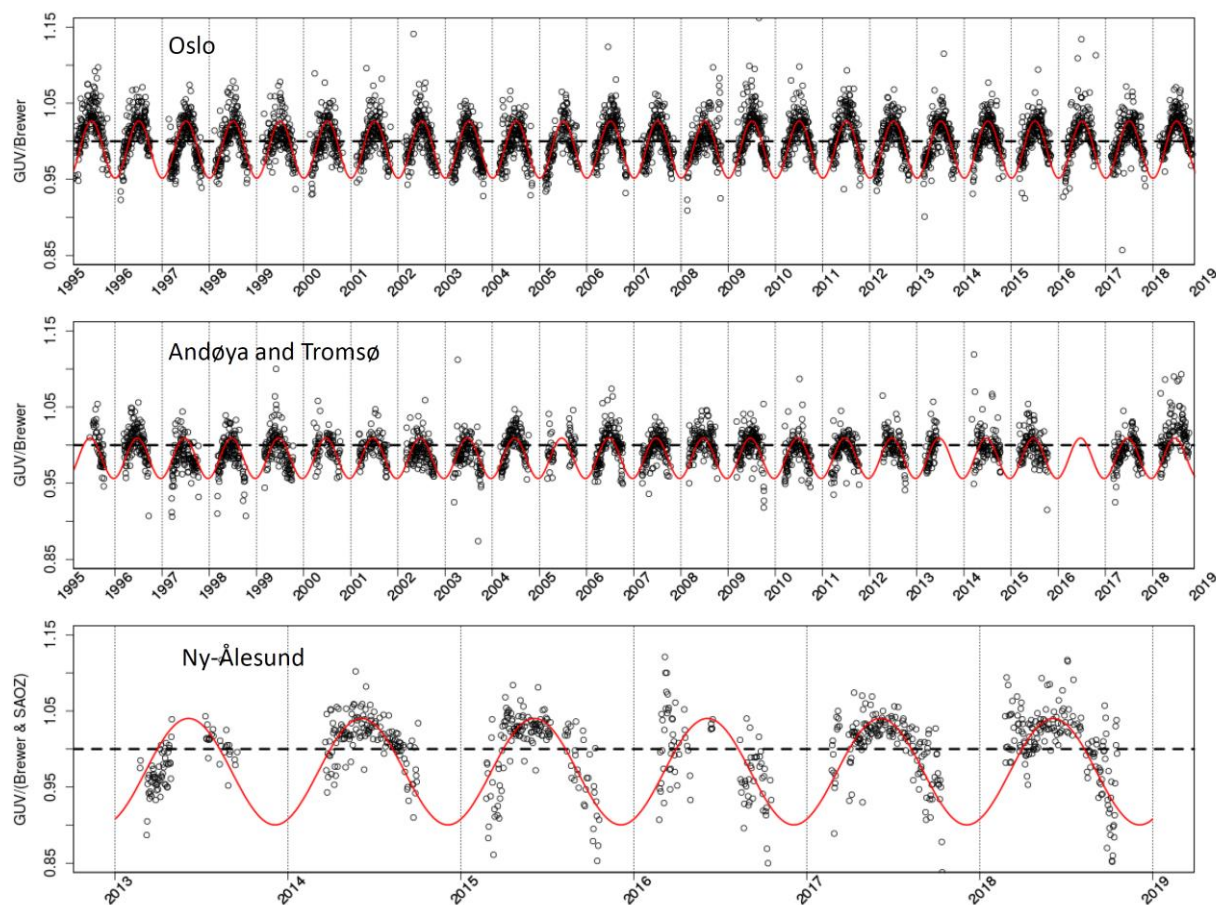
189 As described above, each GUV instrument has a unique set of N-tables, and to obtain optimal ozone measurements it is possible
190 to switch between various tables depending on season and solar zenith angle. However, in our study we have only used one
191 N-table for a given station (with TOMS V7 ozone climatology (McPeters et al., 1996) and 320/305 nm channel ratio) to



192 simplify the ozone estimates and avoid artifacts in trends and statistics generated by lookup table (N-table) changes. To account
193 for possible seasonal errors in total ozone related to the above-mentioned inaccuracies in the atmospheric profile and variations
194 in surface albedo (snow/ice on the ground), we have homogenized the GUV measurements with respect to Brewer Direct Sun
195 (DS) measurements. The Norwegian Brewer instruments have been calibrated by the International Ozone Service (IOS,
196 Canada) every year since installation in the 1990s, except from the summer 2020 when the calibration was prohibited under
197 the covid-19 restrictions. These frequent calibrations are done to ensure high quality Brewer measurements in Oslo/Kjeller
198 (B42) and Tromsø/Andøya (B104) and to make sure that the instruments are well maintained. The instrument B42 in Oslo is
199 an MKV single-monochromator Brewer, which might be influenced by stray-light (Karppinen et al., 2015). We have therefore
200 only used Brewer DS data with ozone slant column below 1100 DU where the effect of stray light is negligible. All Brewer
201 DS data from Oslo/Kjeller and Andøya are available at the World Ozone and Ultraviolet Radiation Data Centre (WOUDC,
202 <https://woudc.org/>). Also, the Italian Brewer (B50) in Ny-Ålesund has been calibrated regularly by IOS Canada, last time in
203 2018, which showed that the instrument has been stable since the previous calibration in 2015. However, there are limited
204 Brewer DS measurements available in Ny-Ålesund and the measuring season is relatively short due to the high latitude (79°N).
205 Thus, in addition to Brewer DS data we have used SAOZ measurements to obtain quality assured ozone data from the early
206 spring and fall. SAOZ derives total ozone from the Chappuis bands in the visible spectrum through the Differential Optical
207 Absorption Spectroscopy (DOAS) method (Pommereau and Goutail, 1988) and contrary to Brewer it can only measure ozone
208 when the solar beam pathway through the atmosphere is large (solar zenith angle > 85°), i.e. around sunrise and sunset.
209 Analyses and QC of the SAOZ data are performed at LATMOS (France) in the frame of the SAOZ global network
210 (<http://saoz.obs.uvsq.fr/index.html>). In this study we have used SAOZ daily average total ozone on days where both sunrise
211 and sunset measurements are available. The data are stored in the Network for the Detection of Atmospheric Composition
212 Change (NDACC) data base (<http://www.ndaccdemo.org/>).

213
214 Figure 2 shows the GUV/Brewer DS ratio for the period 1995-2018 for days with available GUV and Brewer DS (and SAOZ)
215 data. The GUV daily average total ozone values are calculated as 1h averages around local noon, and to limit possible errors
216 caused by clouds we have selected days where the noontime average eCLT from GUV is larger than 60%. Comparisons
217 between GUV (global sky) and Brewer DS time series in Figure 2 demonstrate highly consistent results, i.e. the individual
218 instruments have maintained stable and homogenous since the start in 1995.

219



220

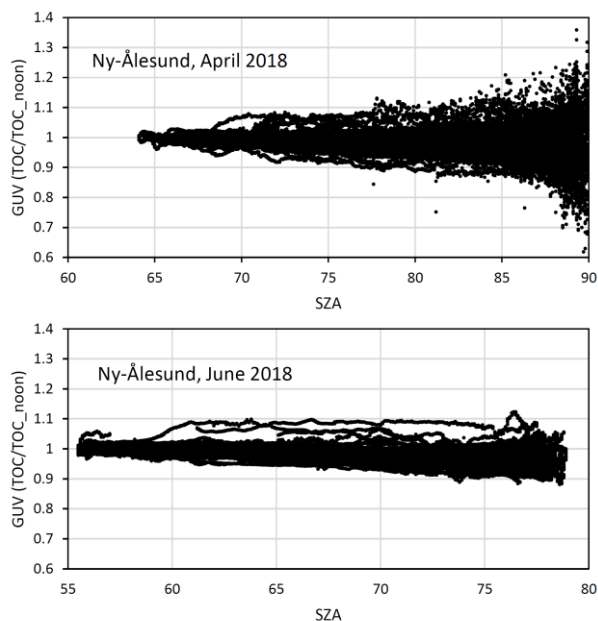
221 **Figure 2: Ratios of GUV/Brewer(DS) ozone values measured in Oslo (top), Tromsø/Andøya (center) and in Ny-Ålesund (bottom).**
222 **SAOZ ozone data are also used in Ny-Ålesund. The red curves represent statistical fit functions.**

223

224 As seen from Figure 2 there is a clear seasonality in the ratio. However, inspections of GUV minute values performed
225 throughout a day do not reveal any systematic SZA dependence in total ozone. On some days, TOC is relatively stable during
226 the day, on other days the values increase or decrease towards the morning/evening. Figure 3 shows two examples from April
227 and June 2018, where GUV TOCs in Ny-Ålesund, normalized to noontime TOC (TOC_{noon}), are plotted throughout the day.
228 The plot from April (Figure 3, top panel) does not indicate any obvious SZA dependence in the measurements. There is a
229 significant spread in the ratio as SZA exceeds 82°, mainly due to noise in measurements of the 305 nm channel. Also, spring-
230 time ozone has normally large day-to-day variations and the morning TOC will often differ from the evening value. The bottom
231 panel in Figure 3, from June 2018, indicates a small decrease in TOCs as SZA increases. At SZA=78°, which is the maximum
232 SZA at midnight in Ny-Ålesund in June, the average ratio TOC/TOC_{noon} is 0.97. This is most likely related to the
233 atmospheric profile in the RTM and N-tables used for ozone retrievals.



234



235

236 **Figure 3: GUV TOC from Ny-Ålesund measured throughout two selected periods: April 2018 (upper panel) and June 2018 (lower**
237 **panel).**

238

239 When all measurements and seasons are considered as a whole, no consistent SZA dependence in TOC can be revealed. Thus,
240 we have chosen seasonal corrections of GUV TOC data to harmonize with other ground-based instruments at the stations. The
241 time series of GUV/Brewer DS (and SOAZ) ratios have been fitted by a function $f(t)$ with two harmonic terms:

242

$$f(t) = a + c \cdot \cos(2\pi t) + s \cdot \sin(2\pi t) \quad (4)$$

243

244 Here t is time (day fraction of the year), a defines the average ratio of GUV/Brewer(&SAOZ), and c and s define the annual
245 cycles of the ratio. The values of a , c , and s for the three stations are listed in Table 2.

246

247 **Table 2: Results from statistical fit of GUV/Brewer(&SAOZ) ratio, see Eq(4).**

Station	a	c	s
Oslo	0.9890	-0.0375	-1.11E-03
Andøya/Tromsø	0.9828	-0.0261	4.56E-03
Ny-Ålesund	0.9702	-0.0623	0.0315

248



249

250 The time periods where the spare GUVs at Andøya were used (see section 3.1) are excluded from the plots shown in Figure 2,
251 since these instruments have slightly different responses than the original instrument.

252

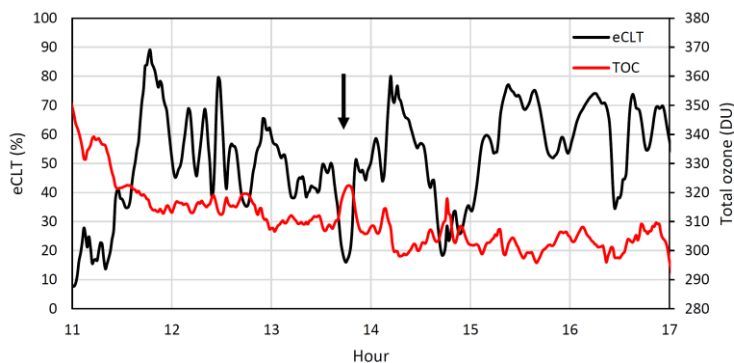
253 The harmonization method described above are applied to the three GUVs operated by NILU, which are co-located with other
254 ground-based ozone monitoring instruments. Total ozone is also derived for the other stations in the UV network (presented
255 in Table 1 and Figure 1), but for these instruments a different approach is used. A description of the method and results will
256 be presented in a separate paper.

257

258 4.2 Ozone cloud correction

259 Under heavy cloud conditions the ozone retrievals are usually less accurate. An extreme example is discussed by Mayer et al.
260 (1998) for a thunderstorm case. They found that multiple scattering caused errors as large as 300 DU. A less extreme situation,
261 which is more representative for Norway, is exemplified in Figure 4. The figure shows eCLT (black line) and total ozone
262 column (red line) derived from GUV measurements in Oslo between 11:00 and 17:00 UTC on 9 September 2018. Figure 4
263 indicates a gradual ozone decrease throughout the day, but what is most interesting is the occurrence of ozone peaks when
264 eCLT is very low. The uncertainty in total ozone increases as the cloud optical depth becomes very large, and normally we
265 use a cutoff at eCLT=20% and do not accept ozone retrievals under these heavy cloud conditions.

266



267

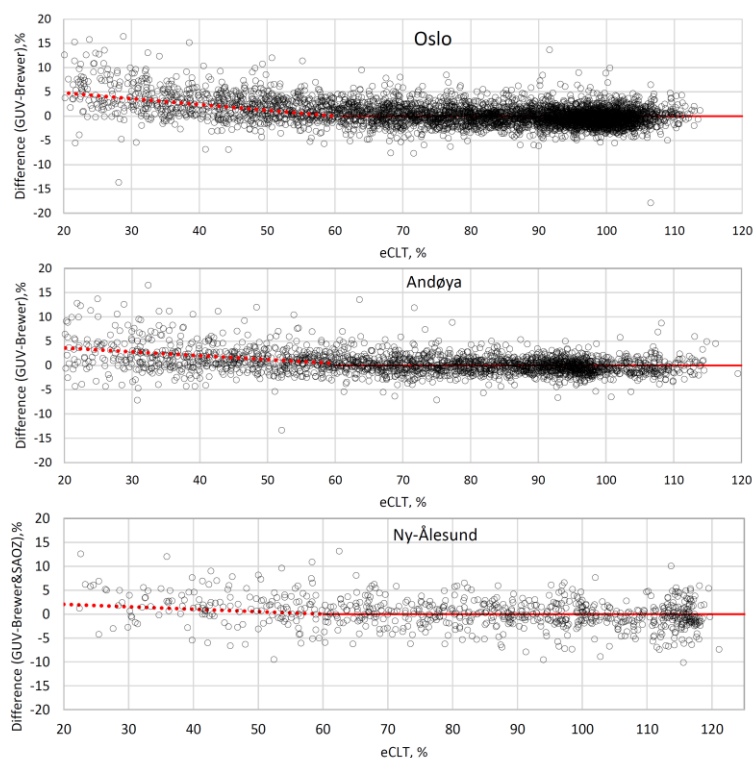
268 **Figure 4: Total ozone and eCLT during a day (9 September 2018) with heavy clouds at Blindern, University of Oslo. Black arrow**
269 **indicates a time where eCLT drops below 20%.**

270

271 The example in Figure 4 shows that total ozone increases by 15 DU (~5%) when eCLT drops from 50% to 16% (see arrow in
272 Figure 4). However, the eCLT effect on ozone is less evident for thinner clouds. In order to examine the impact of clouds on



273 TOC more systematically, we analyzed the percentage difference between Brewer DS (& SAOZ) and GUV noontime total
274 ozone as a function of eCLT, using data starting in 1995. Brewer DS measurements are not performed during cloudy
275 conditions, so these measurements are typically done during a “clear” period the same day as GUV recorded clouds around
276 noon. The results for Oslo, Andøya, and Ny-Ålesund are shown in Figure 5 for observations with $SZA < 80^\circ$. The figure shows
277 that the percentage ozone differences at all the three stations are characterized by gradual decreases for eCLT ranging between
278 20% and 60%, while for $eCLT > 60\%$ the differences do not follow a particular trend and vary around zero.
279



280 **Figure 5: Ozone difference between GUV and Brewer DS (& SAOZ) as a function of eCLT: Oslo (top), Andøya (center) and Ny-**
281 **Ålesund (bottom). The red dotted lines indicate the linear best fitting according to Eq. (5) and Table 3. The presence of eCLT higher**
282 **than 100% is discussed in Section 3.3.**

283 Based on this analysis we have introduced a linear ozone correction (in %) for $eCLT < 60\%$,

284

$$eCLT_{corr} = a * eCLT + b \quad (5)$$

285

286 where a represents the slope and b is a constant. The values of a and b for Oslo, Andøya, and Ny-Ålesund are summarized in
287 Table 3. For Ny-Ålesund there are few Brewer DS and SAOZ data available on days with heavy clouds, and consequently the



288 eCLT correction function is more uncertain than the one for Oslo and Andøya. The overall eCLT correction for Ny-Ålesund
289 is relatively small, i.e. a 2% correction when eCLT drops from 100% to 20%. The corresponding ozone corrections for Oslo
290 and Andøya are ~5% and ~3%, respectively.

291

292 **Table 3: Ozone cloud correction (in %) for eCLT < 60%, a is the slope and b is a constant, see Eq. (5).**

Station	a	b
Oslo	-0.120	7.21
Andøya/Tromsø	-0.0796	4.78
Ny-Ålesund	-0.0515	3.09

293

294 5. Results

295 The full GUV total ozone data from 1995 onwards (Svendby, 2021) have been harmonized with respect to the seasonal
296 correction described in Chapter 4. Specifically, TOCs were divided by the fit-function $f(t)$ in Eq. (4). If the effective cloud
297 transmittance was less than 60% an additional cloud correction, given in Eq. (5), was applied to the data. Accurate GUV total
298 ozone values can be retrieved with this harmonization under most conditions. Analyses of all available GUV and Brewer DS
299 data for the period 1995-2019 give standard deviations of 2.4%, 2.7%, and 4.8% for the GUV-Brewer DS differences for the
300 Oslo, Andøya, and Ny-Ålesund time series, respectively. The standard deviations are reduced to 2.2%, 2.6%, 3.6% if we only
301 include measurements with $SZA < 80^\circ$ and $eCLT > 30\%$. The SAOZ data in Ny-Ålesund are also included in the comparison.
302 Note that the bias between the GUV and Brewer DS time series are close to zero due to the harmonization.

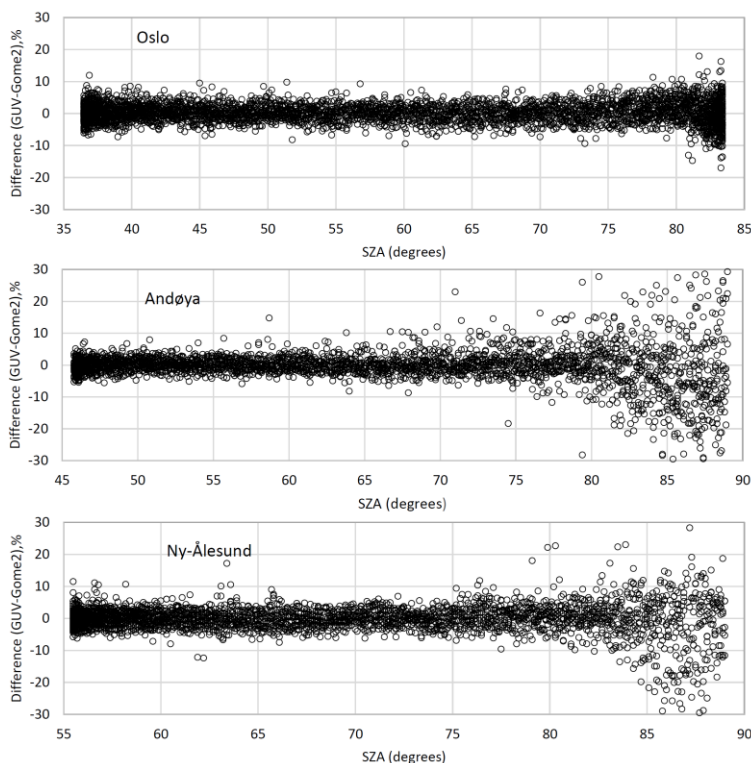
303

304 5.1 Comparison with total ozone column from satellites

305 Corrected GUV TOCs have been compared to Metop-8 GOME2-A TM3DAM v4.1 (Eskes et al., 2003) data for Oslo, Andøya,
306 and Ny-Ålesund. Data from GOME2 is available from 2007. It should be emphasized that GUV data are homogenized with
307 respect to Brewer DS (and SAOZ) data and that any offset between Brewer and GOME2 most likely will be reflected by offset
308 in GUV-GOME2 ozone data. Figure 6 shows the difference (in %) of daily noontime GUV and GOME2 total ozone for the
309 period 2007-2019. Results for Oslo are shown in the top panel, Andøya in the center panel and Ny-Ålesund in the bottom
310 panel. The correlations, biases and STDs are listed in Table 4. At Oslo, the noontime total ozone is never calculated at $SZA >$
311 83° , which is the noontime SZA at the winter solstice. As seen from the figure, the spread in the GUV-GOME2 difference
312 increases as SZA exceeds 82° , especially for the Andøya station. The reason for the larger GUV-GOME2 deviation at Andøya



313 at large SZA is not clear, and it can both be attributed to the GUV instrument retrievals or uncertain satellite measurements at
 314 high SZA in this coastal area with a potentially complex albedo pattern within a single pixel.
 315



316
 317 **Figure 6: GUV-GOME2 total ozone difference: Oslo(top), Andøya (center), and Ny-Ålesund (bottom)**

318
 319 **Table 4: Correlation, bias, and STD in daily noontime GUV-GOME2 total ozone, 2007-2019**

Station	All SZA			SZA<80°		
	Correlation	Bias (DU)	STD (%)	Correlation	Bias (DU)	STD (%)
Oslo	0.977	1.21	3.27	0.982	1.34	2.89
Andøya	0.904	1.31	10.14	0.973	1.49	3.33
Ny-Ålesund	0.961	0.15	4.95	0.985	-0.19	2.76

320
 321
 322 For the period 2007-2019 the overall average difference between GUV and GOME2 is relatively small. The GUV TOC is on
 323 average 1-2 DU (< 1%) higher than the GOME2 TOC for both Oslo and Andøya. As seen in Table 4, the standard deviation



324 (STD) of the GUV-GOME2 differences ranges from 3-10% if all measurements are included. If we only consider
325 measurements with $SZA < 80^\circ$, the STD is ~3% for all stations.

326

327 **5.2 Trends in total ozone**

328 For total ozone assessment and trends studies, the established Brewer instruments would normally be used. However, as
329 demonstrated in previous sections, GUV measurements can provide realistic and stable time series and are suitable for separate
330 trend studies. GUVs that are co-located with a Brewer or another standard TOC instrument for 2-3 years (until harmonization
331 parameters are established), can afterwards be moved to a new location for independent TOC measurements. Data from the
332 GUV instruments are also very useful to extend the measuring season at sites with reduced staff and/or characterized by harsh
333 environmental conditions. The case of Ny-Ålesund, where Brewer data are very sparse due to a rough climate that require a
334 high attendance, is a clear example of GUV usefulness. In Ny-Ålesund as much as 52% of TOC daily means have solely been
335 based on GUV measurements the last five years.

336

337 Even at sites like Oslo and Andøya, where good attendance and less harsh conditions allow more robust Brewer operations,
338 GUV TOC can fill in missing data and extend the measuring season. Brewer zenith sky (ZS) or global Irradiance (GI)
339 measurements (WOUDC 2019) are normally performed under cloudy conditions. However, these measurements can also be
340 prohibited due to high SZA, heavy clouds or technical problems. The last five years, 14% of the daily mean TOC values at
341 Andøya are retrieved from GUV to fill in for missing Brewer DS/ZS/GI measurements.

342

343 The overall GUV data coverage at the Norwegian stations is very good. If we disregard the two calibration campaigns in 2005
344 and 2019, the GUV-511 in Oslo has been in operation ~99% of all days since the start in 1995. Missing days are mainly caused
345 by power failure or minor technical computer issues. TOC retrievals are performed ~95% of all days, where the missing
346 retrievals usually are related to heavy cloud conditions ($eCLT < 20\%$) with high uncertainty. Due to the long and continuous
347 GUV time series, trend analyses based on these data will give a very good picture of the development of the ozone layer above
348 Norway after 1995, along a very wide latitudinal range.

349

350 The GUV network was established during a period where a significant downward trend in total ozone had been observed most
351 places on Earth. Statistical analysis of the Dobson (D56) time series from Oslo 1978-1998 revealed an annual average total
352 ozone decrease of -5.2 ± 0.6 %/decade during this period (Svendby and Dahlback, 2002). For the Norwegian stations, a
353 minimum in annual average total ozone was measured during the period 1993-1997 (Svendby et al., 2020). Thus, a study of
354 trend in GUV total ozone should also consider a possible influence by the low values the first few years.

355



356 Linear trends in the annual average total ozone at the three stations have been calculated, and the results are shown in Figure
357 7: Oslo in the top panel, Andøya in the center panel and Ny-Ålesund in the bottom panel. For the Oslo station we have a full
358 year of data in 1995, whereas the measurements in Tromsø (Andøya) and Ny-Ålesund started in mid-1995 and a full year of
359 data is not available until 1996. Thus 1995 is omitted from the time series at these two stations. Results from the linear
360 regression analyses are presented in Table 5. In addition to trends in annual mean total ozone, the table includes also linear
361 trends for winter (Dec-Feb), spring (Mar-May), summer (Jun-Aug), and fall (Sep-Nov).

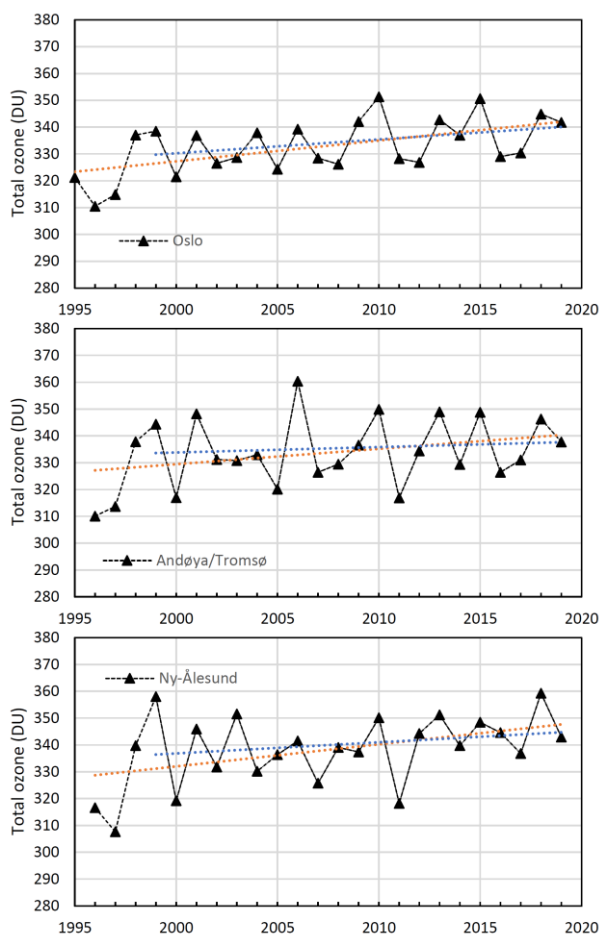
362

363 The annual means in Oslo are based on data from January to December, for Andøya the means are calculated for the months
364 from February to mid-November, whereas data from Ny-Ålesund are based on data from March to October. For the two
365 northernmost stations the winter averages cannot be retrieved because of the polar night. Note also that the fall trend results
366 for Ny-Ålesund, presented in Table 5, do not include November.

367

368 Due to different months included in the Oslo, Andøya and Ny-Ålesund annual means, the absolute values are not comparable.
369 Still, there are many similarities in the three data sets. Even though Oslo and Ny-Ålesund are separated by more than 2000
370 km, the years with low annual average TOC often coincide. The high correlation of 0.7-0.8 between TOC at the three
371 Norwegian sites has mainly a dynamic explanation. Annual variations in dynamically driven ozone transport between warm
372 and cold winters, have a similar impact at all our stations. Also, variations in Quasi-Biennial Oscillation (QBO), El Nino-
373 Southern Oscillation (ENSO), the solar cycle, and stratospheric aerosols will give significant interannual variability in total
374 ozone (WMO 2018; Svendby and Dahlback, 2004). The explanatory variables mentioned above are often used in TOC trend
375 studies to eliminate variability caused by natural sources and to get a more precise picture of trends related to emissions of
376 anthropogenic sources such as ODSs.

377



378

379 **Figure 7: Annual average total ozone in Oslo, at Andøya/Tromsø, and in Ny-Ålesund. Trends for the whole period 1995(96)-2019**
380 **are marked with orange lines, trend for 1999-2019 are in blue.**

381

382 In Figure 7, trends for the entire period (from 1995(96) to 2019) are marked in orange, whereas trends for the last 20 years are
383 marked in blue. The latter trend estimate is done to eliminate the years in the mid-1990s with very low ozone, partly influenced
384 by the Mt. Pinatubo eruption and the cold Arctic winters in 1996 and 1997 (Solomon et al., 1999). The analysis reveals a total
385 ozone increase for the period 1995(96)-2019 at all stations and for all seasons. However, only half of the positive trend results
386 are statistically significant to a 95% confidence level (2σ), that is annual trends in Oslo ($2.3 \pm 1.5\%/decade$) and Ny-Ålesund
387 ($2.4 \pm 2.1\%/decade$), fall trend in Oslo ($3.4 \pm 1.5\%/decade$) and Andøya ($3.0 \pm 2.9\%/decade$), and spring values in Ny-Ålesund
388 ($3.8 \pm 3.4\%/decade$). If we exclude the years 1995-1998 and only look at the trends for the period 1999-2019, the regression
389 analysis still indicates an increase in total ozone during the last two decades. However, the trends are less pronounced and not
390 significant at the 2σ level, except the trend in Oslo ($3.2 \pm 2.0\%/decade$) for fall. The annual TOC trends for the 1999-2019



391 period are 1.5 ± 1.8 %/decade for Oslo, 0.6 ± 2.6 %/decade for Andøya, and 1.2 ± 2.4 %/decade for Ny-Ålesund. Results that
392 are statistically significant are marked in bold in Table 5. Total ozone is strongly influenced by stratospheric circulation and
393 meteorology, which give rise to large interannual variability in total ozone. This variability will reduce the statistical
394 significance and can mask a potential trend in total ozone. The overall positive trend results from the three Norwegian stations
395 agree well with analyses from the “Scientific Assessment of Ozone Depletion: 2018” (WMO 2018). Model simulations
396 presented in WMO (2018) conclude that about half of the observed upper stratospheric ozone increase after 2000 is attributed
397 to the decline of ODSs since the late 1990s. The other half of the ozone increase is attributed to the slowing of gas-phase ozone
398 destruction cycles, which results from cooling of the upper stratosphere caused by increasing concentrations of greenhouse
399 gases. It should be noted that stratospheric cooling reduces Arctic ozone if the temperature drops below the threshold of
400 formation of polar stratospheric clouds (PSCs), as exemplified below. However, PSCs may only exist between December and
401 March and therefore mainly affect ozone trends for winter and early spring.

402

403 **Table 5: Seasonal and annual total ozone trends in Oslo, at Andøya and Ny-Ålesund for the period (a) 1995 – 2019 (start year 1996**
404 **for Andøya and Ny-Ålesund), (b) 1999-2019. Uncertainty is expressed as $2 \times \text{STD}$ (2σ).**

(a) Trend %/decade 1995(96)-2019					
	winter	spring	Summer	Fall	Annual
Oslo	2.90 ± 3.24	1.68 ± 2.28	0.98 ± 1.27	3.37 ± 1.49	2.33 ± 1.47
Andøya		1.36 ± 2.59	0.84 ± 1.38	2.99 ± 2.86	1.70 ± 2.21
Ny-Ålesund		3.82 ± 3.44	0.95 ± 1.27	2.06 ± 4.37	2.44 ± 2.12

(b) Trend %/decade 1999-2019					
	winter	spring	Summer	Fall	Annual
Oslo	1.76 ± 4.02	0.62 ± 2.86	0.70 ± 1.04	3.21 ± 2.00	1.54 ± 1.80
Andøya		-0.33 ± 2.76	0.95 ± 1.52	3.03 ± 3.74	0.59 ± 2.60
Ny-Ålesund		1.39 ± 3.55	0.81 ± 1.54	1.60 ± 5.58	1.23 ± 2.39

405

406

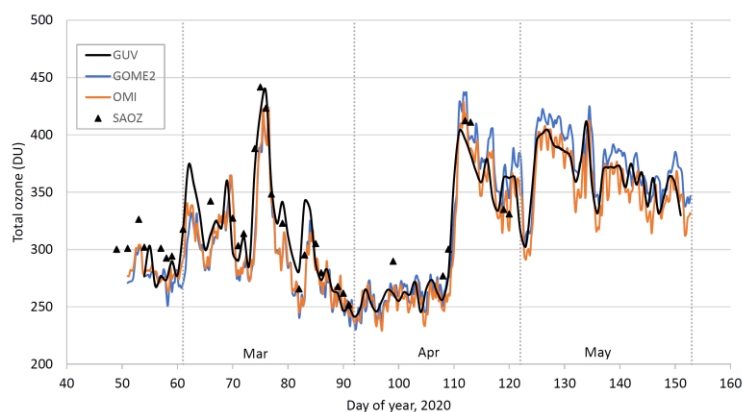
407 Despite a general positive TOC trend, Lawrence et al. (2020) reported that the TOC over the northern polar region was
408 exceptionally small in late winter and early spring 2020. The average total ozone for February to April was the lowest value
409 registered since the start of satellite measurements in 1979. The low TOC was partly caused by an exceptionally cold and
410 persistent stratospheric polar vortex, which provided ideal conditions for chemical ozone destruction (Groß and Müller, 2020;
411 Manney et al., 2020; Wohltmann et al., 2020). These low ozone values resulted in enhanced UV-radiation, and the average
412 UV index measured by the GUV in Ny-Ålesund in April 2020 was elevated by 34% relative to the average 1979–2019 level
413 (Bernhard et al., 2020).

414



415 Figure 8 shows GUV total ozone in Ny-Ålesund from mid-February to May 2020, and the low ozone levels from the end of
416 March to mid-April are clearly seen. Total ozone from SAOZ, GOME2 (TM3DAM v4.1) and OMI (TM3DAM v4.1) are
417 included in the figure for comparison. The study from Wohltmann et al. (2020) showed that the Arctic ozone at 18 km altitude
418 was depleted by up to ~93% in the spring 2020, which is comparable to typical local values in the Antarctic ozone hole. The
419 agreement between GUV, GOME2 and OMI is very good during this ozone loss period, indicating that GUV performs well
420 even though the ozone profile used in the look-up table did not match the actual profile that was observed above Ny-Ålesund
421 in March and April 2020.

422



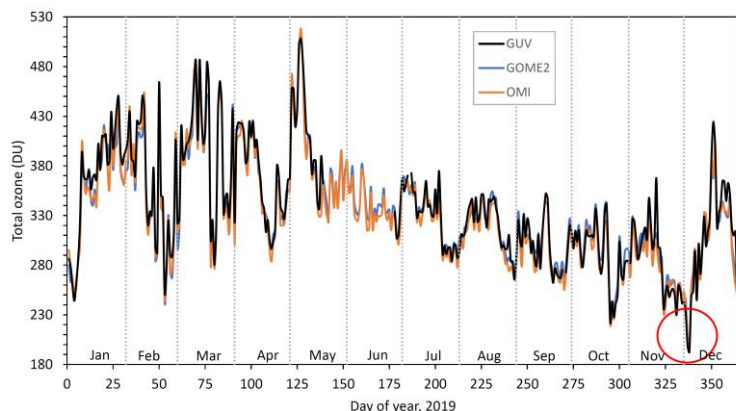
423

424 **Figure 8: Total ozone column measured in Ny-Ålesund the spring 2020 with the SAOZ instrument (black triangles), GUV (black**
425 **line), OMI satellite (orange line) and GOME2 (blue line).**

426

427 Episodes of very low total ozone content are not limited to early spring and periods of several weeks. They can also occur for
428 a few days because of unusual meteorological conditions, as observed at Kjeller in late 2019. In Figure 9, GUV noontime total
429 ozone from Oslo and Kjeller in 2019 is compared to GOME2 and OMI data from Oslo (12:00 values). The black line shows
430 GUV TOC data, whereas blue and orange lines represent GOME2 and OMI measurements, respectively. The lack of GUV
431 data from mid-May and June is caused by the calibration campaign at DSA (see section 3.2). GUV data prior to mid-May 2019
432 are from Oslo, whereas measurements after July 2019 were performed at Kjeller outside Oslo. GUV comparison to GOME2
433 and OMI overpass data from Oslo indicates that the agreement between ground-based measurements and satellite data are as
434 good at Kjeller as in Oslo. A very interesting episode is the extremely low total ozone values measured on 4 December 2019
435 (red circle in Figure 9). On this day, the noontime GUV ozone value at Kjeller was only 193 DU. This is the lowest value ever
436 measured by the GUV in Oslo/Kjeller. GOME2 and OMI from Oslo also measured very low total ozone at 12:00 this day, 201
437 DU and 203 DU, respectively. At 18:00 the previous day the total ozone value from OMI was as low as 193.5 DU.

438

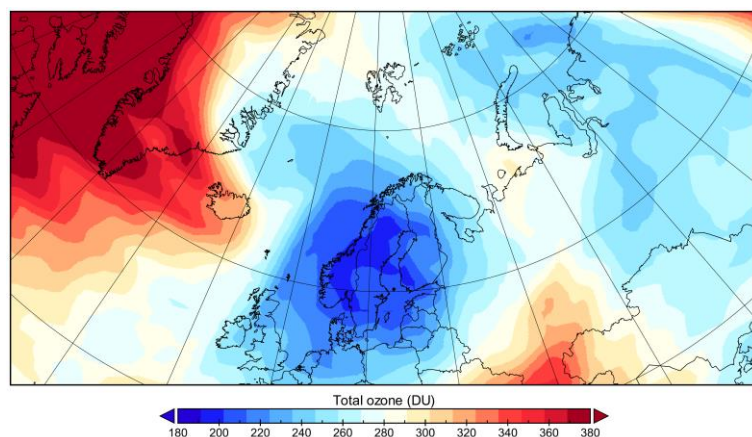


439

440 **Figure 9: Total ozone column values from Oslo/Kjeller in 2019 measured with the GUV instrument (black line), OMI satellite**
441 **(orange line) and GOME2 (blue line). The red circle indicates the mini “ozone hole” over Scandinavia 4 December 2019.**

442 The low total ozone values can be explained by the Arctic polar vortex forming earlier than usual in the fall/winter of 2019
443 (Manney et al., 2020, Lawrence et al., 2020). From the end of November onward, it was cold enough to give rise to PSCs,
444 which were visible over Norway during a large part of the winter 2019/2020. In the area of the vortex, air masses were cut off
445 from ozone supply from lower latitudes, and the “ozone hole” over Southern Norway on 4 December 2019 was possibly caused
446 by both dynamics and photochemical ozone loss. Figure 10 shows total ozone from the GOME2-A satellite at 12:00 this day.
447 As seen from the Figure the TOC was below 200 DU in the middle parts of Norway, Northern Sweden, and South-Western
448 Finland.

449



450

451

452 **Figure 10: Total ozone column on 4 December 2019 at 12:00 from the GOME2-A satellite (data downloaded from**
453 **http://www.temis.nl/protocols/o3field/o3field_msr2.php)**

454

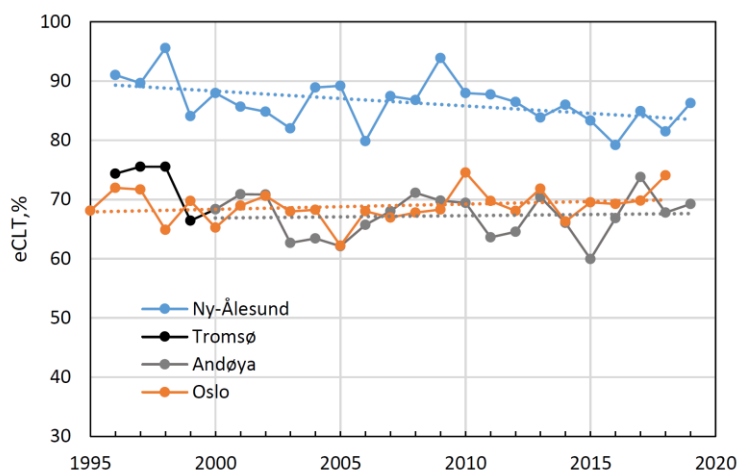


455 5.3 Trends in eCLT

456 As described in Section 3, the effective cloud transmittance (eCLT) expresses the effect of clouds, aerosols and surface albedo
457 on the UV radiation reaching the ground. In the present study an eCLT of 100% represents a clear sky with no surface
458 reflection. An eCLT value above 100% can occur in case of scattered clouds and/or enhanced surface reflection, e.g. snow.

459
460 Figure 11 shows annual average noontime eCLT values and trends at the three stations: Oslo (orange line), Andøya/Tromsø
461 (grey/black line) and Ny-Ålesund (blue line). Linear regression analyses indicate that there are no trends in eCLT at Oslo or
462 Andøya. However at Ny-Ålesund, eCLT has decreased over the last 25 years and a negative trend of ~5% is evident from
463 Figure 11. The change in eCLT is even more pronounced if we only consider the months from late spring and early summer
464 (Apr-Jun), as shown in Figure 12. For these three months the overall decreases in eCLT are ~15% for March and April and
465 9% for June. The decadal trend is -7.6, -7.2, and -3.6 % for April, May, and June, respectively (Table 6).

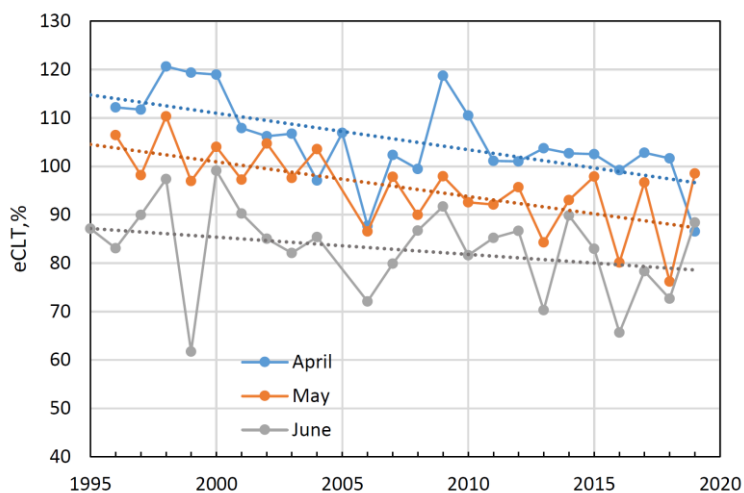
466



467

468 **Figure 11: Annual average noontime eCLT measured in Oslo, Tromsø/Andøya, and in Ny-Ålesund from 1995(96) to 2019. Trends**
469 **in eCLT are indicated as dotted lines.**

470



471

472

473

Figure 12: Monthly mean eCLT in Ny-Ålesund for April, May, and June 1995(96) to 2019. Trends in eCLT are indicated as dotted lines.

474

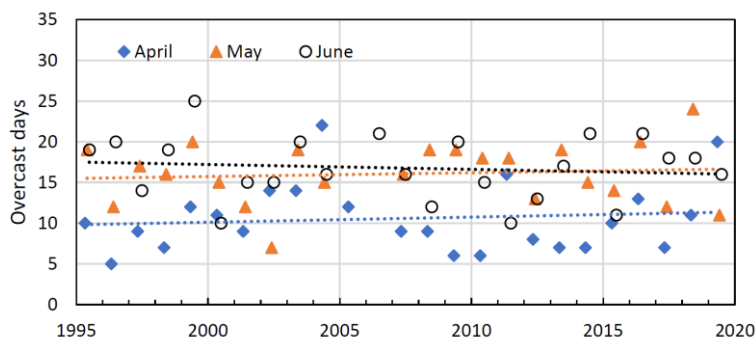
475

To examine possible monthly differences and changes in the cloud cover in Ny-Ålesund for the period 1995-2019, cloud data from the Norwegian Centre for Climate Services (NCCS) has been downloaded (<https://klimaservicesenter.no>). The data describe the number of overcast days observed every month. Cloud observations are performed three times a day, and the fraction of clouds is specified as a number (NN) ranging from 0 to 8. NN=0 means clear sky, whereas NN=8 means completely overcast. If the sum of NNs at 06:00, 12:00, and 18:00 is equal or larger than 20, the day is classified as overcast.

478

479

480



481

482

483

Figure 13: Number of monthly overcast days observed in Ny-Ålesund in April, May, and June 1995 to 2019. Trends in overcast days are indicated as dotted lines. Data are from the NCCS database.

484

485

486

Figure 13 shows the number overcast days for April (blue), May (orange) and June (black) for the period 1995-2019. The average number is ~11 days for April and ~16 days for May and June. Naturally, there are some variations from one year to



487 another, but for the period 1995-2019 as a whole there are insignificant changes/trends in the number of overcast days. In April
488 and May there is an average increase of one overcast day, whereas there is a reduction of one day for June. There is a negative
489 correlation of -0.5 to -0.6 between eCLT from GUV and the number of overcast days from the NCCS data (see last column of
490 Table 6), but it should be noted that eCLT from GUV is based on noontime values, whereas the cloud data from NCCS
491 represent cloud cover for a whole day. Also, a thin cloud cover might be classified as overcast in the NCCS data set, but the
492 eCLT measured by GUV can still be relatively high. Thus, a very high correlation between the two cloud products is not
493 expected.

494

495 **Table 6: Effective cloud transmittance (eCLT) in Ny-Ålesund 1996-2019. “All data” represent monthly noontime average eCLT**
496 **where all days are included. “Clear-sky data” is monthly eCLT noontime average for days with eCLT>100%. Last column is**
497 **correlation between eCLT (all data) and overcast days from NCCS. Uncertainty is expressed as 2*STD (2σ).**

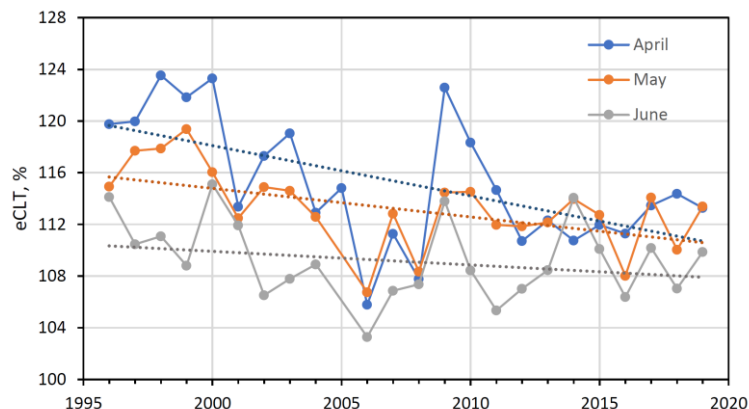
Month	GUV eCLT, all data			GUV eCLT, clear-sky data			GUV and NCCS correlation
	1996-2000 avg, %	2015-2019 avg, %	Trend ± 2σ %/dec.	1996-2000 avg, %	2015-2019 avg, %	Trend ± 2σ %/dec.	
April	116.6	98.5	-7.6 ± 4.3	121.7	112.9	-3.9 ± 2.5	-0.52
May	103.2	89.9	-7.2 ± 3.8	117.2	111.7	-2.3 ± 1.6	-0.64
June	86.2	77.6	-3.6 ± 5.3	111.9	108.8	-1.1 ± 1.8	-0.52

498

499

500 The cloud data from NCCS might partly explain why the overall eCLT is higher for April than May. However, the data cannot
501 explain the decreasing GUV eCLT trend from 1996 - 2019. To examine whether the eCLT trends are related to albedo changes,
502 clear sky data (defined as noontime eCLT ≥ 100%) have been selected from the GUV time series and studied separately.
503 Results are shown in Figure 14. Note that data from April and May 2005 are missing due to the FARIN calibration campaign
504 (see section 3.2). In a similar way as in Figure 12, we can see a clear negative eCLT trend for April and May.

505



506

507 **Figure 14: Monthly mean clear-sky eCLT in Ny-Ålesund for April, May, and June 1996 to 2019. Trends in clear-sky eCLT are**
508 **indicated as dotted lines. There are no data from May and June 2005 due to calibration campaign at DSA.**

509

510 Theoretical calculations (Degünther et al., 1998; Degünther and Meerkötter, 2000; Lenoble, 2000) show that surface ultraviolet
511 irradiance measurements may be influenced by albedo variations more than 10-20 km away. Kylling and Mayer (2001) showed
512 that for Tromsø, Norway, a declining snowline in mountainous areas may have about a 25% (50%) effect on cloudless (cloudy)
513 surface irradiance measurements. These findings support the suggestion that the eCLT trends in Ny-Ålesund are due to albedo
514 changes. The changes can be attributed to local snow/ice conditions, but also to ice/snow changes several kilometers away
515 from the measuring site.

516

517 Clear-sky eCLT mean values and trends from the GUV are summarized in Table 6. The average clear-sky eCLT for April
518 1996-2000 is 121.7%, whereas the April average for 2015-2019 is 112.9%, a reduction of ~9% (-3.9 ± 2.5 %/decade). For May
519 we can see a similar tendency with decreasing clear-sky eCLT of -2.3 ± 1.6 %/decade. The results imply that there has been a
520 significant change in albedo with reduction of snow/ice in the Svalbard area throughout the last 25 years, especially for the
521 spring months. Related results were found by Bernhard (2011) who showed that the onset of snowfall at Barrow, Alaska,
522 advanced by almost 2 weeks/decade for the period 1991-2011. Also, albedo studies from Möller and Möller (2017) has
523 demonstrated a significant negative albedo trend of the glaciers of Svalbard over the period 1979-2015, and data from the
524 Norwegian Polar Institute shows that the sea-ice extent in April in the Barents Sea has considerably declined the last decades
525 (Norwegian Polar institute, 2020). These findings on Arctic albedo change and ice melt clearly support existing reports and
526 publications on ongoing climate change (Wunderling et al., 2020; IPCC 2018).

527



528 **6. Conclusions**

529 The Norwegian UV network has been in operation for 25 years, and the unique GUV data can be used to derive a broad range
530 of atmospheric and biological exposure parameters, including total ozone column (TOC), UV index, and cloud transmittance.
531 The instruments are relatively simple to operate and maintain and measure continuously throughout the day with 1-minute
532 time resolution.

533
534 The 25-year long records of GUV TOC measurements in Norway have been re-evaluated and harmonized. For the three
535 stations located in Oslo, at Andøya and in Ny-Ålesund there are annual TOC increases of 2.3 ± 1.5 %/decade, 1.7 ± 2.2
536 %/decade, and 2.4 ± 2.1 %/decade, respectively, for the period 1996-2019. However, TOC is strongly influenced by
537 stratospheric circulation and meteorology, and the large interannual variability reduces the statistical significance of the data.

538
539 GUV measurements of effective cloud transmittance (eCLT) in Ny-Ålesund, Svalbard, reveal a negative eCLT trend for the
540 spring, indicating that the albedo in the Arctic has decreased over the past 25 years. This is most likely a consequence of an
541 ongoing Arctic ice melt caused by increased temperatures in the Svalbard area.

544 **Data availability**

545 Harmonized GUV TOC and eCLT data: <http://doi.org/10.5281/zenodo.4446609> (Svendby, 2021).

546 Brewer DS data: <https://woudc.org/>

547 SAOZ data: <http://www.ndaccdemo.org/>

548 GOME2-A TM3DAM v4.1: http://www.temis.nl/protocols/o3field/overpass_gome2a.php

549 OMI TM3DAM v4.1: http://www.temis.nl/protocols/o3field/overpass_omi.php

551 **Author contribution**

552 TMS designed the study and performed the analyses. BJ, AD, AK, and GHB performed supporting simulations and analyses.
553 BP and VV provided Brewer#50 data. GHH was responsible for SAOZ data. TMS wrote the paper, and all authors provided
554 input on the paper for revision before submission.

556 **Competing interests**

557 The authors declare that they have no conflict of interest.

559 **Acknowledgement**



560 We thank the Norwegian Environment Agency for funding total ozone and UV measurements in Oslo/Kjeller, Andøya and
561 Ny-Ålesund.

562 References

- 563 Anderson, G. P., Clough, S. A., Kneizys, F. X., Chetwynd, J. H., Shettle, E. P.: AFGL atmospheric constituent profiles (0–
564 120 km),” AFGL-TR-86-0110 Air Force Geophysics Laboratory, Hanscom Air Force Base, Mass., 1987.
- 565 Bernhard, G., Booth, C. R., Ebrahimian, J. C.: Real-time ultraviolet and column ozone from multichannel ultraviolet radiometers
566 deployed in the National Science Foundation's ultraviolet monitoring network. *Optical Engineering*, 44(4), 041011-1 -
567 041011-12, 2005.
- 568 Bernhard, G.: Trends of solar ultraviolet irradiance at Barrow, Alaska, and the effect of measurement uncertainties on trend
569 detection, *Atmos. Chem. Phys.*, 11, 13029–13045. doi:10.5194/acp-11-13029-2011, 2011.
- 570 Bernhard, G., Dahlback, A., Fioletov, V., Heikkilä, A., Johnsen, B., Koskela, T., Lakkala, K., Svendby, T.: High levels of
571 ultraviolet radiation observed by ground-based instruments below the 2011 Arctic ozone hole. *Atmos. Chem. Phys.*, 13,
572 10573-10590. doi:10.5194/acp-13-10573-2013, 2013.
- 573 Bernhard, G., Arola, A., Dahlback, A., Fioletov, V., Heikkilä, A., Johnsen, B., Koskela, T., Lakkala, K., Svendby, T.,
574 Tamminen, J.: Comparison of OMI UV observations with ground-based measurements at high northern latitudes. *Atmos.*
575 *Chem. Phys.*, 15, 7391-7412. doi:10.5194/acp-15-7391-2015, 2015.
- 576 Bernhard, G., Fioletov, V. E., Groöß, J.-U., Ialongo, I., Johnsen, B., Lakkala, K., Manney, G. L., Müller, R., Svendby, T. :
577 Record-Breaking Increases in Arctic Solar Ultraviolet Radiation Caused by Exceptionally Large Ozone Depletion in 2020,
578 *Geophys. Res. Lett.*, 47(24), doi: 10.1029/2020GL090844, 2020.
- 579 Dahlback, A., Stamnes, K.: A new spherical model for computing the radiation field available for photolysis and heating at
580 twilight, *Planet. Space Sci.* 39, 671–683, 1991.
- 581 Dahlback, A.: Measurements of biologically effective UV doses, total ozone abundances, and cloud effects with multichannel,
582 moderate bandwidth filter instruments, *Appl. Opt.* 35, 6514–6521, 1996.
- 583 Degünther, M., Meerkötter, R., Albold, A., Seckmeyer, G.: Case study on the influence of inhomogeneous surface albedo on
584 UV irradiance, *Geophys. Res. Lett.*, 25, 3587-3590, 1998.
- 585 Degünther, M. and Meerkötter, R.: Influence of inhomogeneous surface albedo on UV irradiance: effect of a stratus cloud, *J.*
586 *Geophys. Res.*, 105, 22755-22761, 2000.
- 587 Eskes, H., van Velthoven, P., Valks, P., Kelder, H.: Assimilation of GOME total ozone satellite observations in a three-
588 dimensional tracer transport model, *Q.J.R.Meteorol.Soc.* 129, 1663-1681, doi:10.1256/qj.02.14, 2003.
- 589 Groöß, J.-U., and Müller, R.: Simulation of the record Arctic stratospheric ozone depletion in 2020, Submitted to *J. of Geophys.*
590 *Res.* for the special collection "The exceptional Arctic stratospheric polar vortex in 2019/2020: causes and consequences",
591 doi:10.1002/essoar.10503569.1, 2020.



- 592 Høiskar, B.A.K., Braathen, G.O., Dahlback, A., Bojkov, B.R., Edvardsen, K., Hansen, G., Svenøe, T. : Monitoring of the
593 atmospheric ozone layer and natural ultraviolet radiation. Annual report 2000. Kjeller, NILU, Report 833/01, TA-
594 1829/2001, NILU OR, 35/2001, 2001.
- 595 Høiskar, B.A.K, Haugen, R., Danielsen, T., Kylling, A., Edvardsen, K., Dahlback, A., Johnsen, B., Blumthaler, M., Schreder,
596 J.: Multichannel moderate-bandwidth filter instrument for measurement of the ozone-column amount, cloud transmittance,
597 and ultraviolet dose rates. *Appl. Opt.*, 42, 3472-3479. doi:10.1364/ao.42.003472, 2003.
- 598 IPCC (2018): Global warming of 1.5°C. An IPCC Special Report on the impacts of global warming of 1.5°C above pre-
599 industrial levels and related global greenhouse gas emission pathways, in the context of strengthening the global response
600 to the threat of climate change, sustainable development, and efforts to eradicate poverty [V. Masson-Delmotte, P. Zhai,
601 H. O. Pörtner, D. Roberts, J. Skea, P.R. Shukla, A. Pirani, W. Moufouma-Okia, C. Péan, R. Pidcock, S. Connors, J. B. R.
602 Matthews, Y. Chen, X. Zhou, M. I. Gomis, E. Lonnoy, T. Maycock, M. Tignor, T. Waterfield (eds.)],
603 <https://www.ipcc.ch/sr15/>
- 604 Johnsen, B., Kjeldstad, B., Aalerud, T.N., Nilsen, L.T., Schreder, J., Blumthaler, M., Bernhard, G., Topaloglou, C., Meinander,
605 O., Bagheri, A., Slusser, J.R., Davis, J.: Intercomparison and harmonization of UV index measurements from multiband
606 filter radiometers, *J. Geophys. Res.*, Volume 113, doi:10.1029/2007JD009731, 2008.
- 607 Johnsen, B., T. Svendby, and A. Dahlback: Norwegian UV Network - minute data (Version v1.0.0), Zenodo,
608 doi:10.5281/zenodo.4043039, 2020.
- 609 Karppinen, T., Redondas, A., García, R. D., Lakkala, K., McElroy, C.T., Kyrö, E.: Compensating for the Effects of Stray Light
610 in Single-Monochromator Brewer Spectrophotometer Ozone Retrieval, *Atmosphere-Ocean*, 53:1, 66-73, doi:
611 10.1080/07055900.2013.871499, 2015.
- 612 Kylling, A., and Mayer, B.: Ultraviolet radiation in partly snow covered terrain: Observations and three-dimensional
613 simulations, *Geophys. Res. Lett.*, 28, 3665-3668, 2001.
- 614 Lakkala, K., Kujanpää, J., Brogniez, C., Henriot, N., Arola, A., Aun, M., Auriol, F., Bais, A. F., Bernhard, G., De Bock, V.,
615 Catalfamo, M., Deroo, C., Diémoz, H., Egli, L., Forestier, J.-B., Fountoulakis, I., Garcia, R. D., Gröbner, J., Hassinen, S.,
616 Heikkilä, A., Henderson, S., Hülsen, G., Johnsen, B., Kalakoski, N., Karanikolas, A., Karppinen, T., Lamy, K., León-Luis,
617 S. F., Lindfors, A. V., Metzger, J.-M., Minvielle, F., Muskatel, H. B., Portafaix, T., Redondas, A., Sanchez, R., Siani, A.
618 M., Svendby, T., and Tamminen, J. (2020): Validation of TROPOMI Surface UV Radiation Product, *Atmos. Meas. Tech.*,
619 13, 6999–7024, <https://doi.org/10.5194/amt-13-6999-2020>, 2020.
- 620 Lapeta, B., Engelsen, O., Litynska, Z., Kois, B., Kylling, A.: Sensitivity of surface UV radiation and ozone column retrieval
621 to ozone and temperature profiles, *J. Geophys. Res.*, 105, 5001-5007, 2000.
- 622 Lawrence, Z. D., Perlwitz, J., Butler, A. H., Manney, G. L., Newman, P. A., Lee, S. H. , Nash, E. R.: The Remarkably Strong
623 Arctic Stratospheric Polar Vortex of Winter 2020: Links to Record-Breaking Arctic Oscillation and Ozone Loss, *J.*
624 *Geophys. Res.: Atmos.*, doi:10.1029/2020jd033271, 2020.



- 625 Lenoble, J.: Influence of the environment reflectance on the ultraviolet zenith radiance for cloudless sky, *Appl. Opt.*, 39, 4247-
626 4254, 2000.
- 627 Manney, G. L., N. J. Livesey, M. L. Santee, L. Froidevaux, A. Lambert, Z. D. Lawrence, L. F. Millán, J. L. Neu, W. G. Read,
628 M. J. Schwartz, and R. A. Fuller: Record-low Arctic stratospheric ozone in 2020: MLS observations of chemical processes
629 and comparisons with previous extreme winters, *Geophys. Res. Lett.*, 47(16), doi:10.1029/2020gl089063, 2020.
- 630 McPeters, R. D., Bhartia, P. K., Krueger, A. J., Herman, J. R.: *Nimbus-7 Total Ozone Mapping Spectrometer (TOMS) Data*
631 *Products User's Guide*, NASA Reference Publication, 1996.
- 632 Mayer, B, A. Kylling, S. Madronich and G. Seckmeyer: Enhanced Absorption of UV Radiation due to Multiple Scattering in
633 Clouds: Experimental Evidence and Theoretical Explanation, *J. Geophys. Res.* 103, 31,241-31,254, 1998.
- 634 Möller, M., and R. Möller, R.: Modeling glacier-surface albedo across Svalbard for the 1979–2015 period: The HiRSvaC500-
635 a data set, *J. Adv. Model. Earth Syst.*, 9, 404–422, doi:10.1002/2016MS000752, 2017.
- 636 Norwegian Polar Institute (2020). Sea ice extent in the Barents Sea in April. Environmental monitoring of Svalbard and Jan
637 Mayen (MOSJ). URL: <http://www.mosj.no/en/climate/ocean/sea-ice-extent-barents-sea-fram-strait.html>, 2020.
- 638 PMOD/WRC: Qasume site Audits, URL: <https://www.pmodwrc.ch/en/world-radiation-center-2/wcc-uv/qasume-site-audits/>.
639 Protocol of the intercomparison at DSA, URL:
640 https://www.pmodwrc.ch/wcc_uv/qasume_audit/reports/2019_05_norway_olso.pdf, 2019.
- 641 Pommereau, J.P., Goutail, F.: O₃ and NO₂ ground-based measurements by visible spectrometry during Arctic winter and
642 spring 1988, *Geophys. Res. Lett.* 15, 8, 891-894, 1988.
- 643 Schmalwieser, A.W, J. Gröbner, M. Blumthaler, B. Klotz, H. De Backer, D. Bolsée, R. Werner, D. Tomsic, L. Metelka, P.
644 Eriksen, N. Jepsen, M. Aun, A. Heikkilä, T. Duprat, H. Sandmann, T. Weiss, A. Bais, Z. Toth, A.M. Siani, L. Vaccaro,
645 H. Diémoz, D. Grifoni, G. Zipoli, G. Lorenzetto, B.H. Petkov, A. Giorgio di Sarra, F. Massen, C. Yousif, A.A. Aculinin,
646 P. den Outer, T. Svendby, A. Dahlback, B. Johnsen, J. Biszczuk-Jakubowska, J. Krzyscin, D. Henriques, N. Chubarova,
647 P. Kolarž, Z. Mijatovic, D. Groselj, A. Pribulova, J. R.M. Gonzales, J. Bilbao, J.M.V. Guerrero, A. Serrano, S. Andersson,
648 L. Vuilleumier, A. Webbat, J. O'Haganau (2017) UV Index monitoring in Europe, *Photochem. & Photobio. Sci.*, 16, 1349–
649 1370, doi: 10.1039/c7pp00178a, 2017.
- 650 Solomon, S.: Stratospheric ozone depletion: a review of concepts and history, *Rev. Geophys.*, 37, 275,
651 doi:10.1029/1999RG900008, 1999.
- 652 Stamnes, K., Tsay, S.-C., Wiscombe, W, Jayaweera, K.: Numerically stable algorithm for discrete-ordinate-method radiative
653 transfer in multiple scattering and emitting layered media. *Appl. Opt.*, 27(12), 2502-2509, doi: 10.1364/AO.27.002502,
654 1988.
- 655 Stamnes, K., Slusser, J., Bowen, M.: Derivation of total ozone abundance and cloud effects from spectral irradiance
656 measurements,” *Appl. Opt.* 30, 4418–4426, 1991.
- 657 Stamnes, K., Thomas, G.E., Stamnes, J.J.: *Radiative Transfer in the Atmosphere and Ocean* (Cambridge University, 2017)



- 658 Svendby, T. M., and A. Dahlback: Twenty years of revised Dobson total ozone measurements in Oslo, Norway. *J. Geophys.*
659 *Res.*, 107, 4369, doi: 10.1029/2002JD002260, 2002.
- 660 Svendby, T. M., and A. Dahlback: Statistical analysis of total ozone measurements in Oslo, Norway, 1978-1998. *J. Geophys.*
661 *Res.*, 109, D16107, doi:10.1029/2004JD004679, 2004.
- 662 Svendby, T.M., Hansen, G.H., Bäcklund, A., Nilsen A.-C.: Monitoring of the atmospheric ozone layer and natural ultraviolet
663 radiation. Annual report 2019. Kjeller, NILU, M-1768/2020, ISBN: 978-82-425-3008-0, ISSN: 2464-3327, 2020
- 664 Svendby, T.M.: GUV total ozone column and effective cloud transmittance from three Norwegian sites 1995-2019 (Version
665 v1.0) [Data set]. Zenodo. <http://doi.org/10.5281/zenodo.4446609>, 2021.
- 666 Sztipanov, M., Tumeh, L., Li, W., Svendby, T., Kylling, A., Dahlback, A., Stamnes, J., Hansen, G.H., Stamnes, K.: Ground-
667 based measurements of total ozone column amount with a multichannel moderate-bandwidth filter instrument at the Troll
668 research station, Antarctica, *Appl. Opt.*, 59, 97–106, doi: 10.1364/AO.59.000097, 2020.
- 669 WOUDC (2019): WOUDC Contributor Guide (Version 2.1.3), URL: <https://guide.woudc.org/en/>
- 670 WMO (2008), Johnsen, B., Kjeldstad, B., Aalerud, T.N., Nilsen, L.T., Schreder, J., Blumthaler, M., Bernhard, G., Topaloglou,
671 C., Meinander, O., Bagheri, A., Slusser, J.R., Davis, J.: Intercomparison of global UV index from multiband filter
672 radiometers: Harmonization of global UVI and spectral irradiance. GAW report no. 179 / WMO/TD-No. 1454. Geneva:
673 World Meteorological Organization, 2008.
- 674 WMO (2018): Scientific assessment of ozone depletion: 2018. Geneva, World Meteorological Organization (Global Ozone
675 Research and Monitoring Project-Report No. 58). URL: <https://www.esrl.noaa.gov/csd/assessments/ozone/2018/>, 2018
- 676 Wohltmann, I., P. Gathen, R. Lehmann, M. Maturilli, H. Deckelmann, G. L. Manney, J. Davies, D. Tarasick, N. Jepsen, R.
677 Kivi, N. Lyall, and M. Rex: Near complete local reduction of Arctic stratospheric ozone by severe chemical loss in spring
678 2020, *Geophys. Res. Lett.*, doi:10.1029/2020gl089547, 2020.
- 679 Wunderling, N., Willeit, M., Donges, J.F., Winkelmann, R.: Global warming due to loss of large ice masses and Arctic summer
680 sea ice, *Nature communication*, <https://doi.org/10.1038/s41467-020-18934-3>, 2020.